SLURRY-BASED BINDER JETTING OF CERAMIC CASTING CORES

P. Erhard*, W. Volk*, D. Guenther*

*Fraunhofer Institute for Casting, Composite and Processing Technology, Garching, Germany

Abstract

The production of complex sand cores to represent internal contours in castings is typically achieved by powder-based binder jetting. However, a trade-off between the load-bearing capacity during casting and the subsequent removability from the cast part leads to design limitations. Slurry-based binder jetting allows the processing of fine powders and the economical production of sinterable ceramic cores. Its performance, potential, and challenges are presented in the context of the foundry process chain. As drying affects material properties and process efficiency, detailed investigations are carried out to control the properties via drying. Average roughness depths of 1.2 µm and flexural strengths of 25 MPa were achieved using aqueous quartz slurry and appropriate process parameters. By incorporating predetermined breaking lines into the internal geometry of hollow casting core structures, the stress generated during the solidification of the cast metal induces decoring. A promising process chain is outlined for producing efficient, close-contour coolings in high-performance castings and digital code tags for part tracking in foundries.

Keywords: slurry-based binder jetting, 3D printing, foundry, casting cores, ceramics

Introduction

In the binder jetting process, particle material is applied layer-by-layer to a build platform and printed with binder [1]. This highly productive additive manufacturing process enables, among other things, the production of complex casting cores from sand, which are used to represent internal contours in metallic cast components [2]. The process chain of casting utilizing 3D printed molds and cores, also known as multi-step additive manufacturing for foundry applications, is depicted in Figure 1. The mold and core making sub-process involves the steps of binder jetting (selectively printing binder onto a layer of sand), eventually curing (storage at ambient conditions, microwave or oven curing), de-powdering, and mold assembly. After casting, the cores are removed from the casting. The metal part's material properties may be adjusted in a thermal treatment process, and the final dimensions are set by means of mechanical processing (e.g., sandblasting, milling, and grinding).

Nowadays, 3D printing of casting cores is already transferred to series production in the automotive sector [3]. Commercially available printers specially designed for mass production [4], as well as large format machines with printing volumes of up to 4 x 2 x 1 m [6], realize a high level of automation and extremely high production rates [5] compared to alternative additive manufacturing methods.
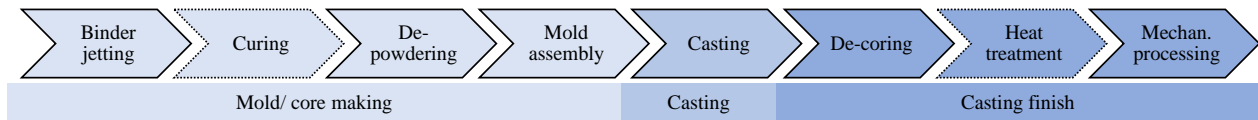
Figure 1. Casting process utilizing 3D printed molds and cores.

However, due to a trade-off between the mechanical and thermal load capacity of casting cores in the casting process and their subsequent release from the cast part, there are technical limitations to the design of cavities in cast components [7]. In the slurry-based 3D printing process, a water-based ceramic slurry is processed instead of dry, flowable silica sand [8]. The suspension-based layer application and the use of fine grain sizes enable high surface qualities and powder bed densities, as well as the production of green bodies whose mechanical properties can be tailored in the subsequent sintering process [9] - an additional process step situated between the 'de-powdering' and 'mold assembly' in the conventional process chain shown in Figure 1. These characteristics are utilizable against the background of the technological requirements for casting cores for high-performance cast components. Filigree, as well as mechanical and thermal stable casting cores that are easily removable from the cast part and a new, innovative process chain in foundries can be realized. By expanding the process knowledge of slurry-based 3D printing with regards to the layer-by-layer drying process that influences both the material properties and the process efficiency, the hurdles for industrial implementation of the technology in the foundry environment are to be lowered.

Materials & Methods

The slurry used in this study consists of ~ 44 vol.-% quartz flour (Sikron SF600, Quarzwerke GmbH, Germany, d_{50} value 3 µm, d_{95} value 10 µm), ~ 55 vol.-% deionized water and ~ 1 vol.-% organic additives (viscosity modulating agent, dispersant, defoamer and preservative). In Vogt et al. [10], the slurry preparation procedure and the rheological properties are depicted in detail, and the sintering process is investigated. A phenolic novolak resin [11] and Hexamethylenetetramine (90/10 wt.-%) dissolved in isopropyl alcohol with a resin-to-solvent ratio of 1/8 is used as the binder system.

Full access to the 3D printing process parameters [12] (Figure 2) is given through a lab-scale test setup for slurry-based 3D printing and appropriate hardware and software components. In previous examinations [12], a coater geometry and process parameters for on-demand coating were developed, ensuring homogeneous layer formation across the build platform and high surface finishes.

The 3D printing process follows the sequence: (1) layer coating at a velocity of 100 mm/s, (2) drying by IR radiation (IRD X230L, Optron GmbH, Germany), (3) lowering of the build platform, and (4) printing onto a layer using a SL 128-AA printhead (Fujifilm Dimatix, Inc., USA). The resulting powder compact containing the test specimens is cured at 280 °C for 1h before clearing the specimens from unprinted regions in a water bath.

Prior to mechanical analysis, specimens are sintered at a sintering temperature of 1,275 °C and a dwelling time of 5 h. The temperature course was optimized to achieve zero net sintering shrinkage by superimposing sintering shrinkage with cristobalite formation, an irreversible phase transition associated with volume expansion in silica polymorphs [13,14].
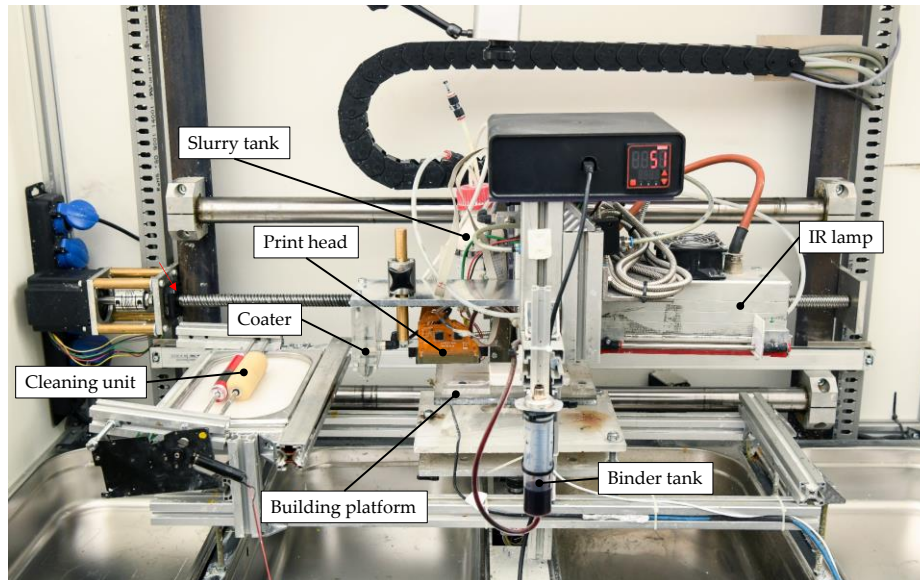
Figure 2. Slurry-based 3D printing test setup. Reproduced under terms of the CC-BY license. [15]

Layer thickness and drying time are central influencing factors on the target parameters microstructure, packing density, strength, and surface quality, which are crucial for casting cores. The layer-by-layer drying of the dispersion medium and the cause-effect chains are investigated using the 3D printing hardware test setup and common material analysis methods for ceramic materials in a full-factorial experimental design. Cuboids measuring 25 x 2.5 x 2 mm (in analogy to DIN EN 843-1, embodiment A [16]) are aligned planar in the printer build volume along the printer axes, with the smallest dimension corresponding to the build direction and the long axis corresponding to the coating direction. The specimens are 3D printed in a quantity of n = 5 and tested for all listed properties. The material characterization methods include:
- Micrographs: BX53M reflected light microscope (Olympus Europa SE & Co. KG, Germany).
- Density (based on DIN EN ISO 18754, method B):
    o Weight: Secura 125-1S analytical balance (Sartorius AG, Germany)
    o Length: caliper gauge (DIN EN ISO 13385-1 [17])
    o Cross-section: micrometer (DIN 863-1 [18])
- Four-point bending strength, elongation at break (based on DIN EN 843-1 [16]): Inspekt table 100 kN universal testing machine (Hegewald & Peschke Meß- und Prüftechnik GmbH, Germany), 5 kN load cell (accuracy class ISO 7500-1 [19]).
- Surface roughness: measurement of specimens' top surface, MarSurf M400 surface measuring instrument (Mahr GmbH, Germany), BFW A 10-45-2/90° probe arm.

The technically relevant process window is determined by conducting 3D printing tests and micrographic examinations. For this purpose, specimens with a layer thickness of 50 and 75 µm

are dried with varying radiated power of 0.73 W/cm², 0.97 W/cm², and 1.18 W/cm², and drying periods between 15 and 75 s. The test specimens are explicitly examined for macroscopic defects.

With these results, the process window is narrowed to a range that allows a stable fabrication of test specimens for extended material analysis. 50 µm layer height specimens are subsequently produced at a radiated power of 0.73 W/cm² and 75 µm layer height specimens at 0.97 W/cm². By determining the appropriate infrared power levels for each layer thickness in advance, drying periods between 15 and 75 s can be investigated in detail.

The results are discussed against the background of state of the art, and an extended fundamental understanding of the process with special attention to the requirements for potential integration into foundry applications is derived. As follows, the prospects of slurry-based 3D printing for advanced casting applications are highlighted in examples of use in the foundry industry. The use case of a high-strength hollow casting core with imprinted predetermined breaking points is used to demonstrate the applicability of the technology for near-contour cooling systems. In a second example, the high resolution and surface quality are used to demonstrate the additive manufacturing of ceramic mold inserts with imprinted digital code tags for traceability purposes.

Control of Material Properties by Means of Drying Configuration

Investigations on the process window precede detailed material analysis. Figure 3 shows exemplary micrographs revealing critical processing parameters. At an IR power density of 1.18 W/cm², which corresponds to the highest investigated drying velocity, the process window is observed to be very narrow: for 50 µm layers, layer casting is feasible at a drying period of only 15 s but not without major defect formation (Figure 3 (b)). The flaws resemble a hat shape, which may originate from inhomogeneous moisture distribution and local warping. During the drying of ceramic suspensions, this effect can occur when the lower part of a layer is saturated with water while the upper part is already subject to shrinkage, forming a dense particle network [20,21]. By drying at a lower IR power density of 0.73 W/cm² (Figure 3 (a)), no defects are observed in the microstructure, and all drying periods were found to be realizable in combination with this precondition. Although not as pronounced as for 50 µm layers, an IR power density of 1.18 W/cm² also leads to a limited process window for 75 µm layers: Figure 3 (c) shows exemplary plate-like defects on a green body produced with a drying period of 15 s. Similar defects can be observed with a drying time of 75 s also. Only when drying for 55 s (Figure 3 (d)) an intact microstructure is achieved. Thus, for subsequent investigations, 50 µm layers are constantly dried with 0.73 W/cm² and 75 µm layers with 0.97 W/cm².

(a) 50 µm layers, layer-by-layer drying at an IR power density of 0.73 W/cm² for 15 s

(b) 50 µm layers, layer-by-layer drying at an IR power density of 1.18 W/cm² for 15 s

(c) 75 µm layers, layer-by-layer drying at an IR power density of 1.18 W/cm² for 15 s

(d) 75 µm layers, layer-by-layer drying at an IR power density of 1.18 W/cm² for 55 s
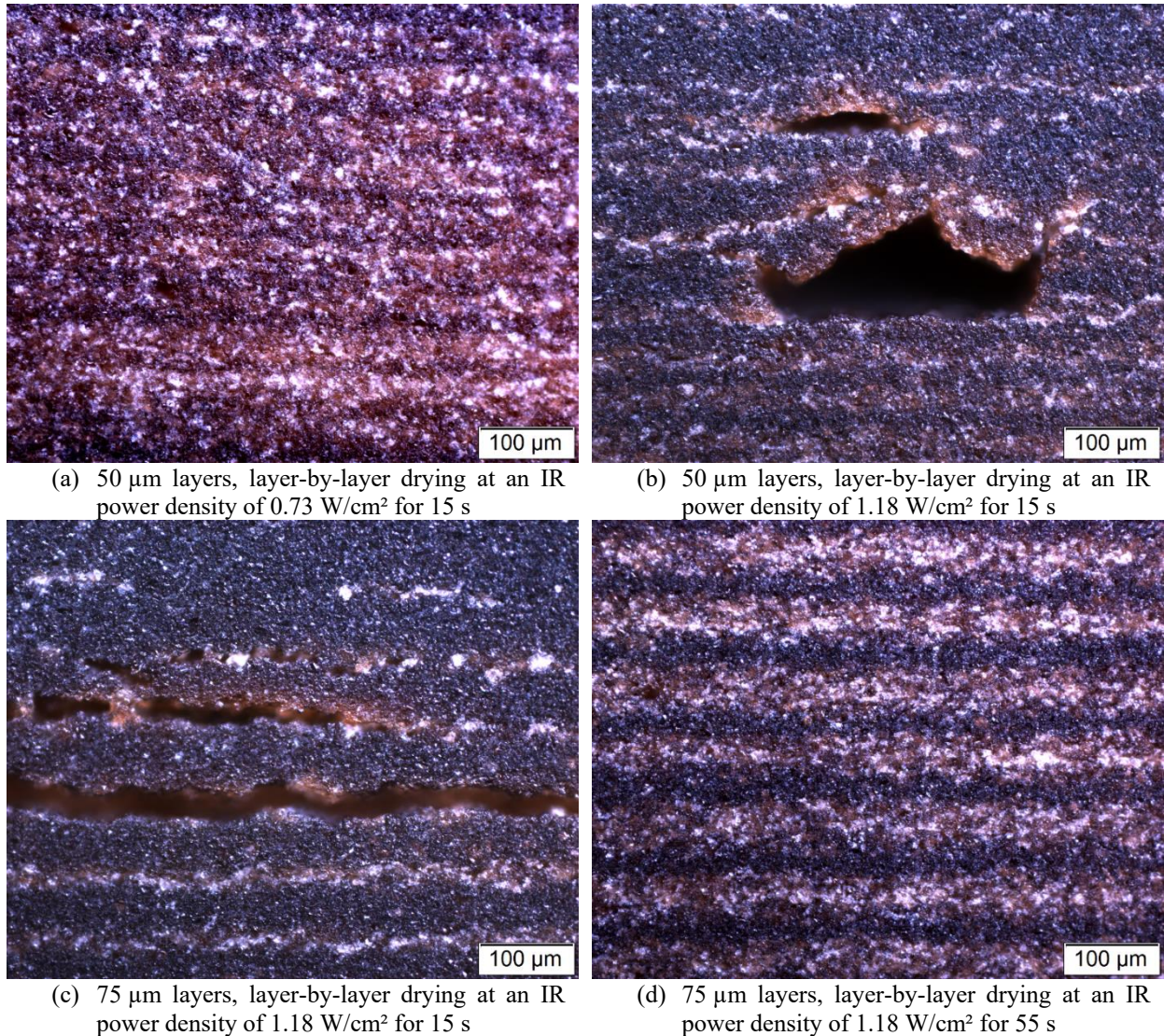
Figure 3. Exemplary micrographs of green body specimens. 50 µm layer specimens dried with a low IR power density of 0.73 W/cm² enable stable layer formation without major defects (a). At an IR power density of 1.18 W/cm² (b)-(d), only 75 µm layers dried for 55 s (d) do not show large defects.

Figure 4 depicts the material analysis results for varying layer thicknesses in a representation of the distributions across all drying durations. In this investigation, the surface roughness Ra is determined on the upper-level plane surface, providing an indication of the maximum achievable surface quality without taking into account the stair-step effect, which depends on the layer thickness. Figure 4 (a) shows higher Ra values and a higher spread for 75 µm layers. It can thus be stated that better surface qualities can be achieved with 50 µm layers compared to 75 µm layers. For comparison with standard material systems used in the foundry industry (e.g., using silica sand with a medium grain size of 0.13 mm, type GS14 RP, Strobel Quarzsand GmbH, Germany), the average roughness depths are found to improve by ~ 90 % using the slurry-based binder jetting method compared to the powder-based alternative.

(a) Specimens' roughness distributions in dependence on the layer thickness.

(b) Specimens' density distributions in dependence on the layer thickness.

(c) Specimens' strength distributions in dependence on the layer thickness.

(d) Specimens' elongation at break distributions in dependence on the layer thickness.
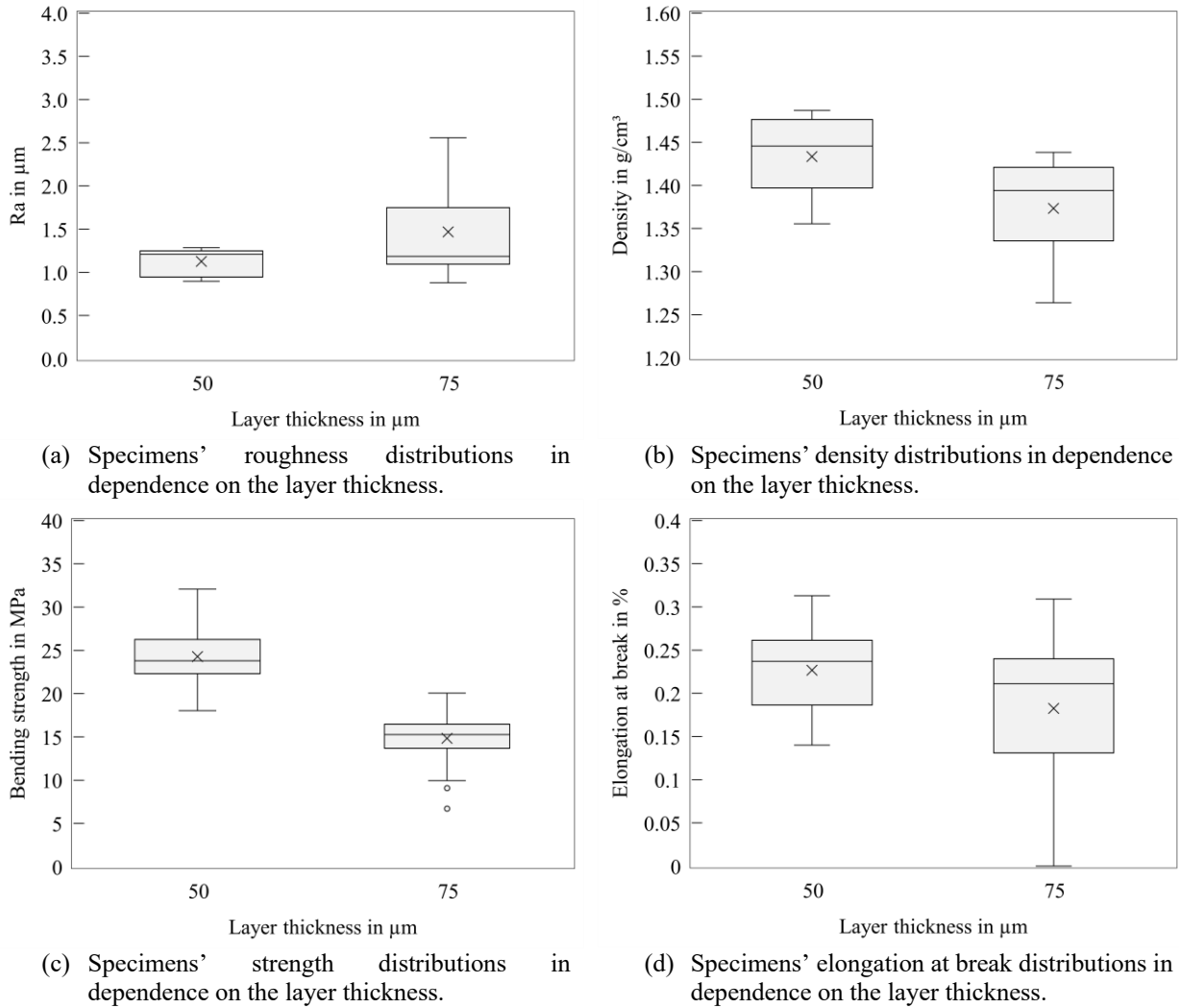
Figure 4. Specimens' material properties in dependence on the layer thickness. With an increased layer thickness, the surface roughness Ra (a) increases, and the density (b), four-point bending strength (c), and elongation at break (d) decrease.

As expected, the mechanical properties of four-point bending strength and elongation at break correlate with the packing density. Due to the fact that pores and cracks concentrate stress, the size of the failure-inducing defect and the probability of appearance are decisive for failure during mechanical testing of brittle ceramic materials [22,23]. The results indicate that the process control leads to a rather uniform pore concentration without causing pore agglomeration or cracks. All aforementioned properties deteriorate with an increased layer thickness. Thinner layers are regarded as favorable in technical aspects since improved compaction through capillary forces and homogeneous low-stress drying are facilitated.

Figure 5 shows the development of the specimens' material properties with increasing drying periods exemplary for 75 μm layer specimens. The respective values for the 50 μm specimens propagate similarly. The plane-level average surface depth Ra (Figure 5 (a)) is found to decrease with increasing drying periods. Low drying times are suspected to cause too high residual

moisture levels within the layer. High moisture contents below a partially dried top surface may lead to an enhanced risk of tearing open the top layer. The density (Figure 5 (b)) increases with increasing drying periods until a drying period of 35 or 55 s, while the mechanical properties (Figure 5 (c),(d)) also improve until a drying period of 55 s is reached. It is shown that by applying exceedingly high drying periods above 55 s, the material properties deteriorate. This may be due to increasing temperatures of an underlying layer that may cause rapid solidification instead of controlled capillary flow during casting of a new layer and thus inhibit compaction.
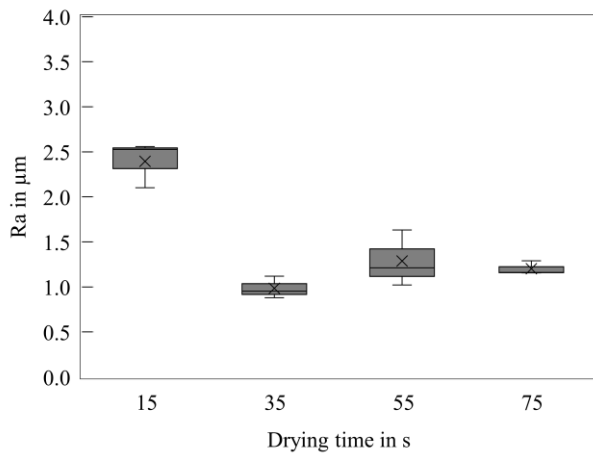
(a) Specimens' roughness distributions in dependence on the drying time for 75 µm specimens.
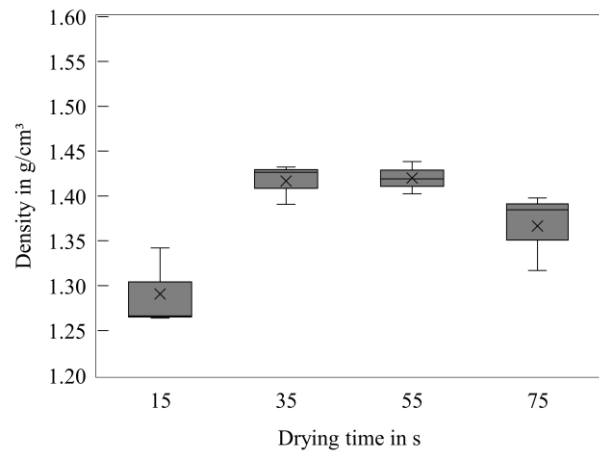
(b) Specimens' density distributions in dependence on the drying time for 75 µm specimens.
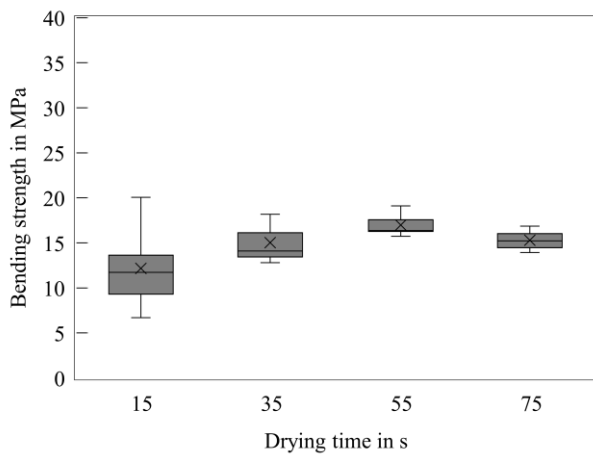
(c) Specimens' strength distributions in dependence on the drying time for 75 µm specimens.
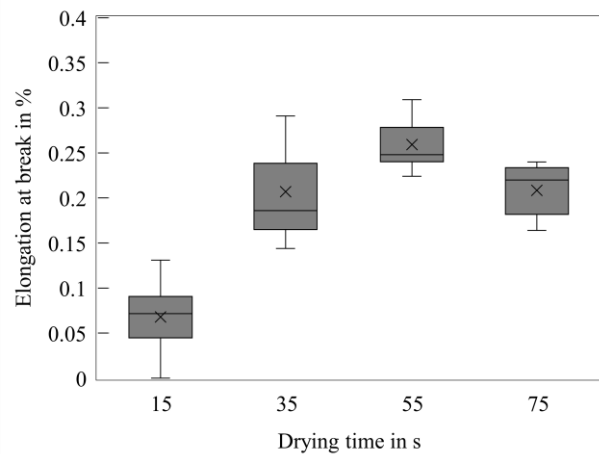
(d) Specimens' elongation at break distributions in dependence on the drying time for 75 µm specimens.

Figure 5. Specimens' material properties in dependence on the drying time. With longer drying, the surface roughness Ra (a) decreases. Density (b), four-point bending strength (c), and elongation at break (d) increase until a drying period of 55 s. By applying exceedingly high drying periods above 55 s, the material properties deteriorate.

Prospects for Advanced Casting

The properties of casting molds and cores have a strong influence on the properties of the castings - especially in the area immediately adjacent to the mold surface - and on the process design. By exploiting the advantages of the slurry-based binder jetting process, new possibilities open up for the design of cavities in castings. The most important technological benefits of slurry-based 3D printed ceramic casting cores over conventional sand cores for foundry applications include:

- High surface quality
- High strength, adjustable during sintering
- High temperature stability

The main drawback is the reduced productivity and energy demand through drying the slurry's solvent and the subsequent sintering process. However, by drawing full benefit from the aforementioned outstanding material properties, new opportunities for advanced casting applications arise.

The design of cooling channels in electric motor housings is of utmost importance with respect to the achievable efficiency [24,25]. Filigree, complex, and self-supporting ceramic core geometries fabricated by slurry-based binder jetting may enable the production of highly efficient liquid-cooled electric motors with complex water flow system designs via casting technology. In the aerospace industry, temperature-stable, high-strength ceramic cores produced by stereolithography or injection molding are employed in investment casting, e.g., for the manufacture of internally cooled airfoils. However, their release from the casting is highly laborious and commonly accomplished by leaching [26] - a procedure that is not feasible in most foundry applications from a cost and environmental point of view. By using the additive manufacturing technology presented herein and a process-oriented design developed with the aid of finite element modeling, a filigree hollow casting core (Figure 6 left, diameter 8 mm, wall thickness 1.5 mm) with predetermined breaking lines that withstands the thermal and mechanical loads during casting but fails autonomously as a result of the shrinkage of the solidifying cast metal was realized, and the process limits were demonstrated (Figure 7).

Traceability throughout the entire casting process is of substantial importance for digital manufacturing. The superior surface properties of slurry-based 3D printing can be leveraged by integrating the production of ceramic digital code mold inserts for part tracking in conventional casting processes (Figure 6 right, feature sizes ~ 0.7 mm). With simple cameras and image processing methods, automatic code recognition of slurry-based 3D printed digital tag's imprints in castings, even after heat treatment and sandblasting, is regarded as feasible in future smart foundries.
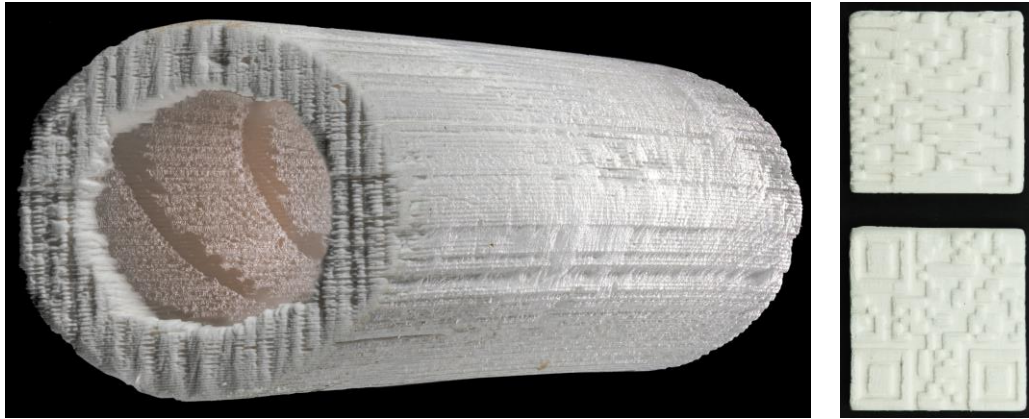
Figure 6. Examples of new applications for advanced casting opened up by slurry-based 3D printing - self-collapsible core (left) and digital code mold inserts for part tracking purposes (right).
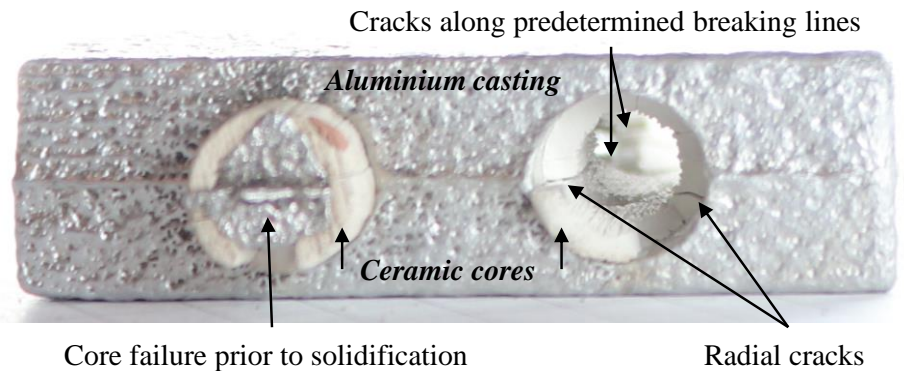
Figure 7. Test casting utilizing cores with predetermined breaking lines – core failure during casting (left), self-collapsibility during solidification of the cast metal (right).

Conclusion

The material properties in slurry-based 3D printing can be controlled by the drying configuration. Lower layer thicknesses and higher drying times were shown to improve density, mechanical strength, ductility, and surface quality. An inverse behavior was observed above a certain degree of drying (drying period > 55 s): overdrying can lead to macroscopic defects. While a reduction in layer thickness and an increase in drying duration are beneficial regarding the material properties, these process parameters are economically disadvantageous as they result in slower build rates. To resolve the conflict of objectives between structural integrity and economic benefits and to ensure both high productivity and advantageous material properties, industrial slurry-based binder jetting machines may provide a large printing area and a drying unit optimized with regard to controlled and efficient moisture removal.

The average roughness depths were reduced by ~ 90 % to 1.2 µm compared to casting cores made from sand-binder systems. In a shrinkage-free sintering process, a four-point bending strength of 25 MPa was set, which is approx. 10 times the value of sand cores. The temperature stability of the cores is ensured by the sintering process preceded by debinding. The high selectivity

of the 3D printing process enabled the integration of predetermined breaking points in the internal geometry of filigree hollow casting cores. With a tailored design, the stresses generated during shrinkage of the solidifying metal alone can induce failure of the ceramic core. This makes mechanical decoring of high-strength ceramic casting cores, such as those required for efficient, close-contour cooling structures in high-performance cast components, possible. The trade-off between the strength of casting cores and their removability from the cast can thus be resolved by exploiting the potentials offered by slurry-based 3D printing and the associated design freedom. By demonstrating the feasibility of slurry-based 3D printed digital code mold inserts, new process-integrated prospects for surface were shown. In the future, multi-material core packages of ceramic mold elements and conventional molded parts made of sand could be used in a cost-effective and sustainable overall process to produce highly complex, function-integrating components.

References

[1] E.M. Sachs, J.S. Haggerty, M.J. Cima, P.A. Williams (Massachusetts Institute of Technology) US5204055 A, 1989.

[2] T. Sivarupan, N. Balasubramani, P. Saxena, D. Nagarajan, M. El Mansori, K. Salonitis, M. Jolly, M.S. Dargusch, A review on the progress and challenges of binder jet 3D printing of sand moulds for advanced casting, Additive Manufacturing 40 (2021) 101889. https://doi.org/10.1016/j.addma.2021.101889.

[3] G. Stegmaier, Neuer 6-Zylinder Biturbo für M3 und M4: Zu 90 Prozent kein BMW-Motor, 2019. https://www.auto-motor-und-sport.de/tech-zukunft/bmw-m3-motor-2020-sechszylinder-biturbo/# (accessed 28 January 2023).

[4] Loramendi S. Coop., Industrialization of Core Printing (ICP), 2023. https://www.foundry-planet.com/d/loramendi-industrialization-of-core-printing-icp/ (accessed 27 June 2023).

[5] P. Erhard, C. Hartmann, R. Li, W. Volk, D. Günther, Advanced Procedures for Series Production with 3D-Printed Core Packages, Inter Metalcast (2023) 1–12. https://doi.org/10.1007/s40962-023-01046-1.

[6] J. Kang, Q. Ma, The role and impact of 3D printing technologies in casting, China Foundry 14 (2017) 157–168. https://doi.org/10.1007/s41230-017-6109-z.

[7] F. Ettemeyer, M. Schweinefuß, P. Lechner, J. Stahl, T. Greß, J. Kaindl, L. Durach, W. Volk, D. Günther, Characterisation of the decoring behaviour of inorganically bound cast-in sand cores for light metal casting, Journal of Materials Processing Technology 296 (2021) 117201. https://doi.org/10.1016/j.jmatprotec.2021.117201.

[8] J.E. Grau, Fabrication of engineered ceramic components by the slurry-based three dimensional printing process. Ph.D., Cambridge, 1998.

[9] S. Diener, H. Schubert, A. Held, N. Katsikis, J. Günster, A. Zocca, Influence of the dispersant on the parts quality in slurry-based binder jetting of SiC ceramics, J American Ceramic Society 105 (2022) 7072–7086. https://doi.org/10.1111/jace.18693.

[10] J. Vogt, M. Stepanyan, P. Erhard, D. Günther, S. Garching, F. Schmalzl, S. Gläser, Slurry-based 3-D-printing of Casting Cores, Casting Plant & Technology (2021) 30–35.

[11] N. Egeler, M. Torbus, M. Knezevic, G. Bae, R. Laitar, D. Trinowski, W. Seelbach (Hüttenes-Albertus Chemische Werke GmbH) EP 2 522 683 A1, 2012.

[12] P. Erhard, A. Seidel, J. Vogt, W. Volk, D. Günther, Evaluation and optimisation of a slurry-based layer casting process in additive manufacturing using multiphase simulations and

spatial reconstruction, Prod. Eng. Res. Devel. 16 (2022) 43–54. https://doi.org/10.1007/s11740-021-01078-8.

[13] L. Pagliari, M. Dapiaggi, A. Pavese, F. Francescon, A kinetic study of the quartz–cristobalite phase transition, IOP Conf. Ser.: Mater. Sci. Eng. 33 (2013) 3403–3410. https://doi.org/10.1016/j.jeurceramsoc.2013.06.014.

[14] C.B. Carter, M.G. Norton, Ceramic Materials: Science and engineering, Springer, New York, 2016.

[15] P. Erhard, J. Angenoorth, J. Vogt, J. Spiegel, F. Ettemeyer, W. Volk, D. Günther, Characterization of Slurry-Cast Layer Compounds for 3D Printing of High Strength Casting Cores, Materials 14 (2021) 6149. https://doi.org/10.3390/ma14206149.

[16] Deutsches Institut für Normung e.V., DIN EN 843-1: Advanced technical ceramics - Mechanical properties of monolithic ceramics at room temperature - Part 1: Determination of flexural strength, Beuth Verlag GmbH, Berlin, 2008.

[17] Deutsches Institut für Normung e.V., DIN EN ISO 13385-1: Geometrical product specifications (GPS) - Dimensional measuring equipment - Part 1: Design and metrological characteristics of callipers, Beuth Verlag GmbH, Berlin, 2020.

[18] Deutsches Institut für Normung e.V., DIN 863-1: Geometrical product specifications (GPS) - Micrometers - Part 1: Micrometers for external measurements; maximum permissible errors, Beuth Verlag GmbH, Berlin, 2017.

[19] DIN EN ISO 7500-1: Metallische Werkstoffe - Kalibrierung und Überprüfung von statischen einachsigen Prüfmaschinen - Teil 1: Zug- und Druckprüfmaschinen - Kalibrierung und Überprüfung der Kraftmesseinrichtung, Beuth Verlag GmbH, Berlin.

[20] G.W. Scherer, Theory of Drying, J American Ceramic Society 73 (1990) 3–14. https://doi.org/10.1111/j.1151-2916.1990.tb05082.x.

[21] M. Murray, Cracking in coatings from colloidal dispersions: An industrial perspective, 2009. https://www.soci.org/-/media/files/conference-downloads/2009/rideal-lectures-apr-09/murray.ashx (accessed 5 March 2022).

[22] D. Munz, Ceramics: Mechanical Properties, Failure Behaviour, Materials Selection, firstst ed., Springer Berlin / Heidelberg, Berlin, Heidelberg, 1999.

[23] C. Zhang, S. Yang, Probabilistic Prediction of Strength and Fracture Toughness Scatters for Ceramics Using Normal Distribution, Materials (Basel) 12 (2019). https://doi.org/10.3390/ma12050727.

[24] F.J. Feikus, P. Bernsteiner, R.F. Gutiérrez, M. Łuszczak, Weiterentwicklungen bei Gehäusen von Elektromotoren, MTZ Motortech Z 81 (2020) 42–47. https://doi.org/10.1007/s35146-019-0180-5.

[25] S. Jahangirian, A. Hassanpour, S. Krishnan, Demagnetization Simulations of High-Power Electric Motors for Reliable Electric Aircrafts, in: AIAA Propulsion and Energy 2020 Forum, VIRTUAL EVENT, American Institute of Aeronautics and Astronautics, Reston, 2020.

[26] W.-J. Zhu, G.-Q. Tian, Y. Lu, K. Miao, D.-C. Li, Leaching improvement of ceramic cores for hollow turbine blades based on additive manufacturing, Adv. Manuf. 7 (2019) 353–363. https://doi.org/10.1007/s40436-019-00273-2.